

SUBSTRUCTURES IN MINOR MERGERS' TIDAL STREAMS

D.A. Noreña,^{1†} J. C. Muñoz-Cuartas,¹ L.F. Quiroga,¹ and N. Libeskind^{2,3}

Received June 27, 2018; accepted July 16, 2019

RESUMEN

En este trabajo se explora si subestructuras como cúmulos estelares se pueden formar del puente de marea producido durante un minor merger. Usamos simulaciones de N-cuerpos y SPH de una galaxia satélite interactuando con su galaxia host. Estudiamos la distribución de masa en los streams para identificar sobredensidades en las que se podrían formar subestructuras. Encontramos que sin gas no se da formación de subestructuras pues ninguna sobredensidad muestra morfología definida ni estabilidad dinámica. Incluyendo gas encontramos la formación de muchos grumos, estructuras longevas físicamente ligadas ($t \geq 1$ Gyr). Analizamos las órbitas, edades y masas de estas estructuras, encontrando una correspondencia con los subsistemas del halo. Concluimos que es posible formar estructuras como cúmulos estelares del material disponible en los puentes de marea y encontramos evidencia en favor de la presencia de materia oscura en esos sistemas.

ABSTRACT

In this work, we explore the idea that substructures like stellar clusters could be formed from the tidal stream produced in galactic minor mergers. We use N -body and SPH simulations of satellite galaxies interacting with a larger galaxy. We study the distribution of mass in streams to identify overdensity regions in which a substructure could be formed. We found that without gas, no substructure formed as none of the overdensities shows a definite morphology nor dynamical stability. Including gas we found that several clumps appear and proved to be real long standing physical structures ($t \geq 1$ Gyr). We analyzed the orbits, ages and masses of these structures, finding its correspondence with the halo subsystems. We conclude that it is possible to form cluster-like structures from the material in tidal streams and found evidence in favour of the presence of dark matter in these systems.

Key Words: galaxies: interactions — galaxies: evolution — galaxies: star clusters — (Galaxy:) globular clusters: general — (Galaxy:) open clusters and associations: general — methods: numerical

1. INTRODUCTION

The galactic halo has plenty of astrophysical systems evolving under the interaction of the different galactic components. These substructures have diverse nature, dynamics and origins and together constitute the building blocks of the ongoing galaxy formation process. Among others, there are many stellar subsystems as the open and globular clus-

ters (Binney & Tremaine 2008), pure gaseous ones as high velocity clouds (HVC) (Wakker & van Woerden 1997) and combined gaseous and stellar systems such as tidal streams and satellite galaxies (Ibata et al. 2001).

Open and globular clusters are segregated by several characteristics. Open clusters are considered as more young, metal rich than their globular counterparts, in addition, open clusters are associated spatially with the galactic disc while globular are mostly distributed spherically all around the halo. This segregation suggest that their formation processes are diverse. In one hand, the formation of open clusters is considered well understood as the collapse

¹FACom - Instituto de Física, FCEN, Universidad de Antioquia (UdeA), Calle 70 No. 52-21, Medellín, Colombia.

²Leibniz-Institut für Astrophysik Potsdam (AIP), An der Sternwarte 16, D-14482 Potsdam, Germany.

³Institut de Physique Nucléaire de Lyon (IPNL), University of Lyon; UCB Lyon 1/CNRS/IN2P3; Lyon, France.

and fragmentation of molecular clouds in the galactic disk (Elmegreen & Efremov 1997). The case of globular clusters exhibits a greater degree of complexity because actually there are two subpopulations of them. There is a metal poor globular cluster population (MPGC) extended across the halo, and the young, metal rich population (MRGC) (Carroll & Ostlie 2006). In addition, there are several cases that do not fit very well in the two previous subpopulations as it is the case of the globular cluster ω -Centauri (henceforth ω -Cen) mainly due to its unusual size and metallicity dispersion (Harris 1999). This variety suggests that even only for the globular clusters there are diverse formation mechanisms.

Different models have been proposed to explain possible formation mechanisms for the two subpopulations of globular clusters in The Galaxy. For the old MPGC subpopulation the widely accepted hypothesis is that they come from primordial density fluctuations in the density field at very high redshift, when the universe expanded and cooled to a temperature of about 4000K and the baryonic density was approximately 10^4 atoms cm^{-3} (Reina-Campos et al. 2019). Under this conditions, the only density fluctuations that can grow with time has wavelength in excess of the critical Jeans length of about 5 pc (Peebles & Dicke 1968).

For the young MRGC subpopulation, several models have been proposed but it appears that there is not a single mechanism that can form all existing MRGC in a given galaxy (Ashman & Zepf 1992; Bekki & Freeman 2003; Shapiro, et al. 2010). One of the main models suggests that a significant fraction of the metal-rich subpopulation may have originated in interacting galaxies, both minor and major mergers (Ashman & Zepf 1992). Major mergers cause several starburst episodes in the gaseous component of each galaxy, and globular clusters can be formed in regions with high gas density (Li et al. 2004). Minor mergers may also contribute to the young population with clusters formed within the small satellite galaxy from the interaction with the larger galaxy (Zepf & Ashman 1993). Also, the globular cluster system of the minor galaxy would eventually be accreted by the largest galaxy, also contributing to the MPGCs subpopulation (Forbes & Bridges 2010). The minor merger scenario can be seen in the Magellanic Clouds, where there is observational evidence of ongoing cluster formation and an ancient cluster system bound to the clouds (Harris 1998; Georgiev et al. 2010). It was further suggested that the very central region of a satellite galaxy could form a globular cluster as the bound structure surviving the effects of

the tidal stripping induced by its host galaxy (Bekki & Chiba 2002).

Moreover, recently observational evidence that suggests that several (if not all) GCs contain various stellar populations has come to light. For example, many GC stars have the same amount of Fe (and other heavy elements) inside a specific radius, but a wide variation in light elemental abundance (Li-Ai) on a star-to-star basis (Conroy et al. 2011). Norris & Kannapan (2011) is a crucial study in this problem; they showed that some ultra-compact dwarf galaxies have color magnitude diagrams indistinguishable from those of GCs and the nuclei of dwarf galaxies. Bekki & Freeman (2003) found that the multiple stellar populations of ω -Cen can be explained in terms of a nucleated dwarf galaxy scenario: the tidal field of the host galaxy induces gas inflow towards the center of the cluster progenitor, triggering multiple star bursts that lead to chemical enrichment. Other GC candidates that are thought to have formed in ostensibly dark matter potential wells deep enough to retain self-enriched Fe produced by supernovae Ia explosions include M22, NGC 1851 and Andromeda's G1. The evidence showing chemical complexity of the cluster stellar populations suggest that the classical picture of all GC's belonging to a single monolithic population should be reevaluated.

Similarly, HVCs appear to be the result of two possible mechanisms: One is the return to the disc of gas and dust expelled via supernovae events and the other is the infall of gas and dust from a stripped subsystem, such as globular clusters or satellite galaxies (Wakker & van Woerden 1997).

A combination of both processes is necessary to explain the current distribution of high and intermediate velocity clouds. For example, from hydrodynamical simulations it is concluded that most massive HVC such as the well known Complex C were originated from ejection of material from the Milky Way's disc (Fraternali et al. 2015); but the velocity dispersion, the metallicity, sizes and masses of the smallest clouds are consistent with an extragalactic origin (Blitz et al. 1999; Binney et al. 2009).

As a result of the tidal disruption of the Galaxy subsystems, the so-called tidal streams are originated. They are composed in most cases by stars and gas (Belokurov et al. 2006), like the Magellanic Stream, where recent observations have confirmed the presence of a young open star cluster most likely formed in the stream (Price-Whelan et al. 2018). Remarkably, all the streams observed in the Milky Way galaxy are clearly nonhomogeneous and exhibit over-

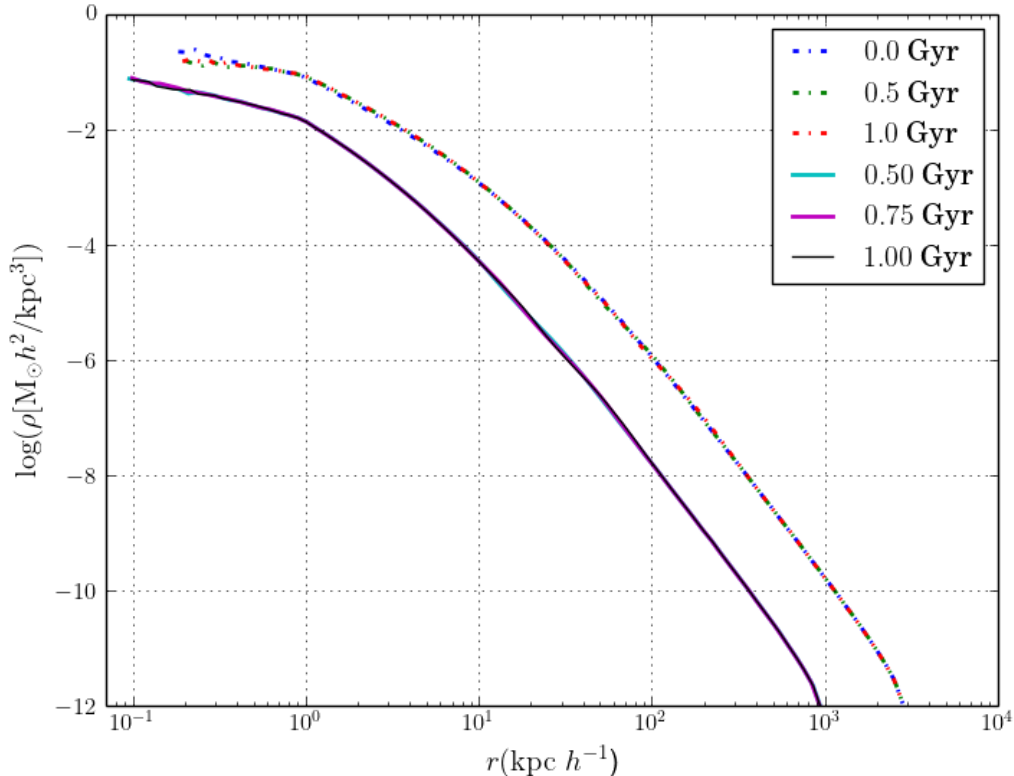


Fig. 1. Convergence of the density profiles of the host (top) and satellite (bottom) dark matter halos under numerical relaxation. The galaxies were evolved isolated for 1 Gyr.

densities (Küpper et al. 2012). These overdensities evolve in the galactic potential as well, undergoing different processes that could eventually transform them into self gravitating systems like clusters. The main purpose of this work is to determine through N -body simulations of galaxy minor mergers if the overdensities in the tidal streams could really meet the conditions to be considered self-gravitating substructures. In a future work, we will investigate under what conditions the evolution of such substructures could lead to the formation of real astrophysical systems such as globular clusters and high velocity clouds.

This paper is organised as follows: In Section 2 we describe the whole setup of the N -body simulations, from the determination of the satellite galaxy initial position to the structure of the host galaxy passing through the astrophysical characteristics of the satellite. In Section 3 we describe the analysis performed to the simulations outputs in order to search and characterise the overdensities. In Section 4 we present our results to finally discuss them and

present the conclusions in Section 5.

2. NUMERICAL PROCEDURES

The numerical setup of the N -body simulations used in this work comprises two stages. In the first instance the galaxies were generated in isolation, in this case, we generate a host disc galaxy and a spheroidal satellite galaxy, both with and without gas. We used these galaxy models to explore different merger configurations. In the following sections we describe in detail each part of the procedure.

We used the code Gadget2 to run all our simulations (details of the code can be found in Springel (2005)). Gadget2 is a general purpose code to study the evolution of collisionless gravitational systems. Collisionless particles representing stars and dark matter evolve only under gravity using a tree method. To follow the evolution of gas an entropy based smoothed particle hydrodynamics (SPH) scheme (Springel & Hernquist 2002) is used with adaptive smoothing lengths, allowing conservation of energy and entropy in adiabatic re-

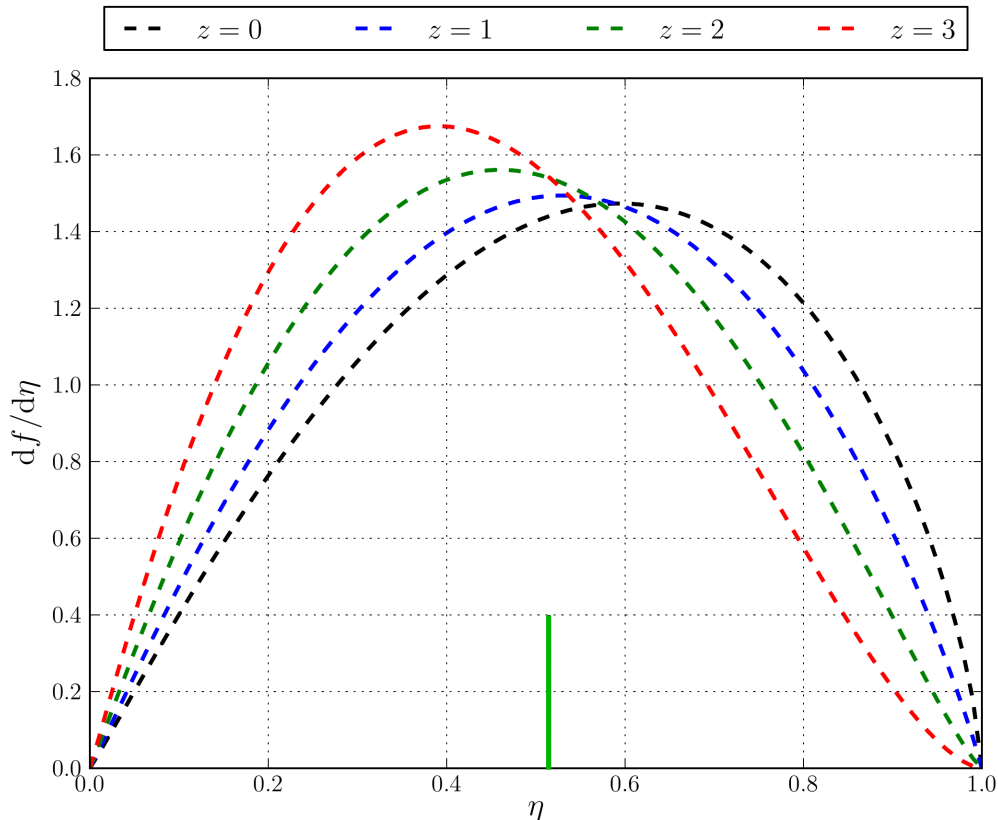


Fig. 2. Circularity distribution for the infalling satellites at different redshifts. The small vertical line indicates the average circularity at $z = 2$.

gions. A synchronization scheme within the integration scheme is used, this is a quasi-symplectic KDK leap-frog with adaptive individual time-steps. The code uses a parallelization algorithm based on a space-filling curve getting high flexibility with high accuracy in tree force estimation.

2.1. Initial conditions

2.1.1. Isolated Galaxies

The host galaxy in this work consists of a disk galaxy composed of a stellar disk and a dark matter halo. Neither gas in the disk nor a central spheroid is included in the model. The satellite galaxy is modelled as a spherical galaxy with a collisionless spheroid hosting a gaseous sphere in hydrostatic equilibrium.

Initial conditions were computed using moments of the collisionless Boltzmann equation (Hernquist 1993; Springel et al. 2004). The dark matter halo of both galaxies follow a Hernquist density profile with scale length parameter adjusted to fit the shape of the NFW density profile as done in Springel (2005).

Masses for the galaxies are taken from the CLUES simulations (Gottloeber et al. 2010; Forero-Romero et al. 2011). The mass of the dark matter halo hosting the disk galaxy is $7.9 \times 10^{11} h^{-1} M_{\odot}$ with a concentration parameter of $c = 4.15$. The satellite galaxy has a total mass of $3.2 \times 10^{10} h^{-1} M_{\odot}$, and $c = 4.26$. Since it is not reasonable to simulate the formation of globular clusters observed today using properties of current host galaxies, the masses and properties of these two progenitor galaxies are related to the properties of the Milky Way galaxy and one of its satellites at $z = 2$ as observed from the constrained simulations made by CLUES. Galaxy disk structure (disk scale length, etc.) is modelled using the prescription of Mo et al. (1998) from which the scale parameters of the disk are $r_d = 1.53$ kpc and $z_0 = 0.31$ kpc.

The host galaxy has a stellar disk with a mass of $3.3 \times 10^9 h^{-1} M_{\odot}$ where we have used Moster et al. (2010) to estimate the total stellar mass for the given dark matter halo at $z = 2$ and assumed that all the

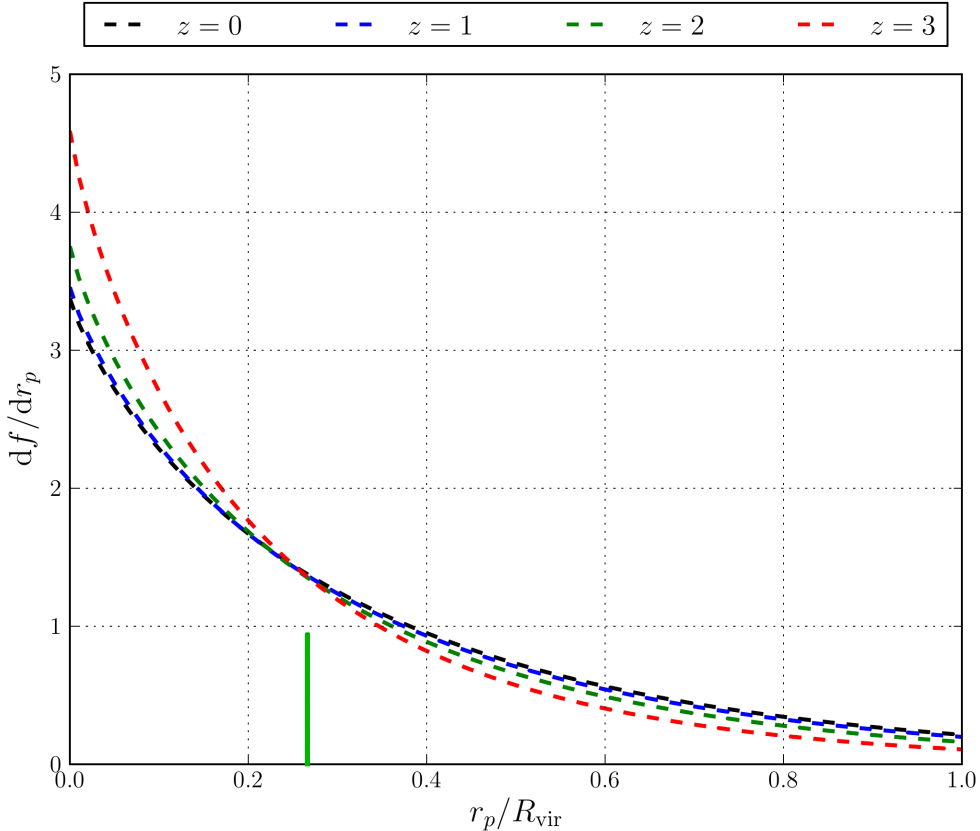


Fig. 3. Pericentre distribution for the infalling satellites; the redshift dependence is explicitly noted. The small vertical line indicates the average pericentric distance value at $z = 2$.

stellar mass is deposited in the disk. Since we are not interested in the evolution of the gas in the disk of the host galaxy and we assume it does not have a dominant effect on the dynamics of the merger, we do not include a gaseous component into this galaxy.

The satellite galaxy is composed of collisionless particles representing dark matter or stars, and has also a gaseous component. Initially, the gas follows a density profile similar to the profile of the dark matter halo in hydrostatic equilibrium. Hydrostatic equilibrium is guaranteed through gas temperature which is computed as Mastropietro et al. (2005)

$$T(r) = \frac{m_p}{k_B \rho_g(r)} \int_r^\infty \rho(r) \frac{GM(r)}{r^2} dr, \quad (1)$$

where m_p is the proton mass, k_B is the Boltzmann constant and $\rho_g(r)$ is the gas mass density. In order to provide a favorable scenario for the formation of clusters from the material deposited in the stream, the total gas mass in the satellite has been chosen to be $\sim 16\%$ of its total mass, providing the

scenario for a gas rich merger. Although arbitrary, the gas fraction is in no way larger than the cosmological baryon fraction in a dark matter halo (Lin, et al. 2008). We could have included a disk of cold gas in to the satellite, however this would have implied a new degree of freedom in our simulations (see next section). Since the direction of the disk may affect the formation of a stream and formation of potential candidates to GCs in our simulations, we decided to go for a simpler spherical distribution looking for a point that is general enough to study the formation of potential GCs in our simulations. We claim that if any structure is formed with this setup, for sure, they can be formed in more favorable conditions where a disk provides cold gas to the stream.

All galaxies are simulated in isolation after the generation of initial conditions in order to allow for numerical relaxation of the initial conditions. Figure 1 shows, for the dark matter halos, the convergence of the profiles from the initial conditions to the final relaxed density profile. Note that the mass dis-

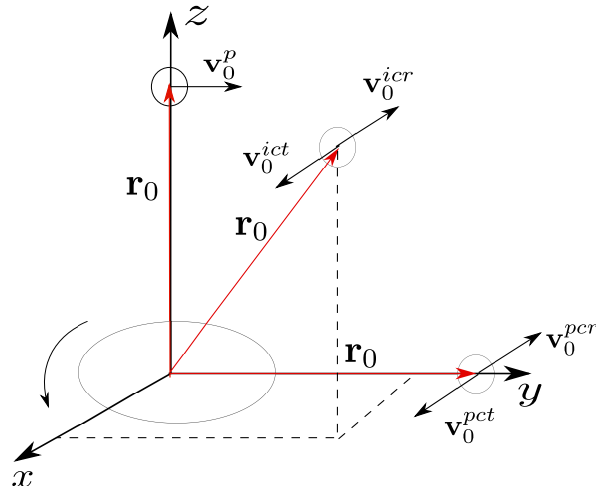


Fig. 4. Schematic representation of the initial orbital configurations for the original five simulations. The host disc is rotating counterclockwise in the $x - y$ plane. \mathbf{r}_0 and \mathbf{v}_0 are the initials position and velocity in each case. For the inclined configurations, the angle with the z axis is $\phi = 45^\circ$. See table 1 for details on the coordinate values.

tribution only changes in the very inner region and after the first 1 Gyr the profile is relaxed. Also, the satellite galaxy reaches relaxation basically very close from the beginning. This check is relevant since it is important to make sure that there is no numerical artificial evolution on the density distribution of the galaxies, since in this way we can ensure that any change in the mass distribution of the system during the merger is due to the dynamics of the merger and is not spurious numerical noise or any instability originated from the initial conditions.

2.1.2. Merger configuration

The mergers we plan to study in this work are somehow artificial in the sense that they do not correspond to the simulation of any realistic system. However these simulations must reproduce the reality of our universe. In that sense, there is an infinite set of possible merger simulations we could run, each with a different orbit. To avoid running many orbits, and at the same time trying to reproduce the expected results from our understanding of the universe, we will use the results shown in Wetzel (2011) to choose the orbits to be studied in this work. In their work Wetzel (2011) study the probability distribution of orbital parameters of infalling satellite galaxies. From them, we use the mean orbital parameters as those of a representative merger that is in agreement with the current cosmological paradigm.

Then, to configure the merger we need to obtain realistic values of the initial position \mathbf{r}_0 and velocity \mathbf{v}_0 of the satellite galaxy. For that, from Wetzel

(2011), we use the circularity η and the pericenter r_p distance that depend on the host halo mass M_{host} and redshift z and that for our host halo mass are distributed at the moment of their passage through the host's virial radius according to the distribution functions shown in figures 2 and 3. In both figures, the mean values of the circularity and the pericentre at $z = 2$ are highlighted with a small vertical green line.

Orbit circularity has a nearly constant small rate of decrease with redshift while pericenter distance exhibits a decrease in its average values with z . In particular, at $z = 2$ we obtain an average pericentric distance of $0.27R_{\text{vir}}$, with R_{vir} the virial radius of the host halo. For this halo $R_{\text{vir}} \approx r_{200} = 63.29$ kpc. The average circularity at $z = 2$ is 0.54. With this two values we calculate the eccentricity e and apocentric distance r_a using the two body approximation as

$$e = \sqrt{1 - \eta^2}, \quad (2)$$

$$r_a = \left(\frac{1 + e}{1 - e} \right) r_p. \quad (3)$$

For our system, the numerical values were found to be $e = 0.84$ and $r_a = 198.34$ kpc. Finally, making use of the *vis-viva* equation, the velocity at apogalacticon is simply

$$v_a = \sqrt{2 \frac{GM}{r_a} (1 - e)}, \quad (4)$$

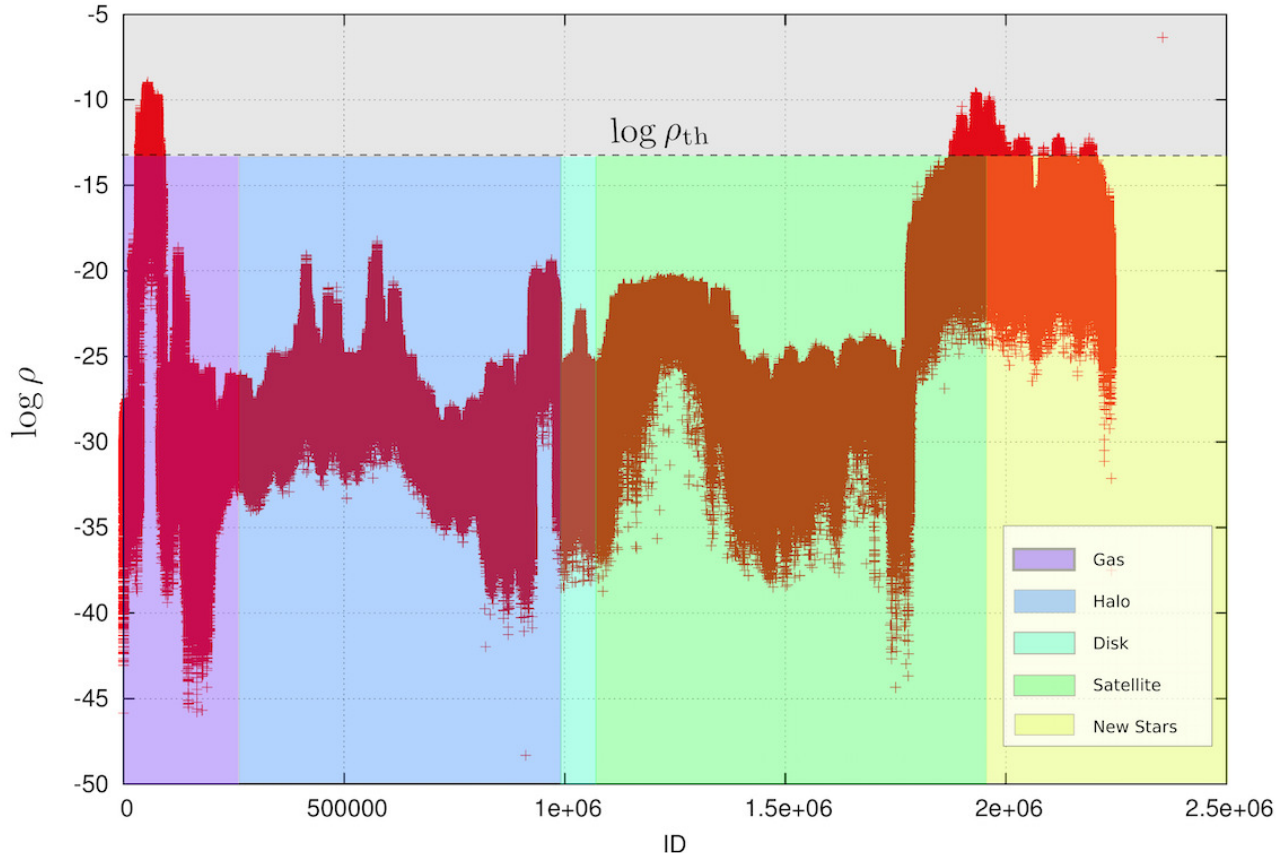


Fig. 5. Density values for the particles in GAS2 p -simulation against the identification particle number. This plot correspond to the snapshot at 3.75 Gyr after simulation starts. Density units are $10^{10} M_{\odot}/\text{kpc}^3$

which turns to be 34.9 km/s for our infalling satellite.

In all simulations the host galaxy disk was always in the $x - y$ plane with its angular momentum aligned with the z -axis. Based on the orbital parameters given in the previous paragraph, the merger was disposed in five different configurations. The only difference between each configuration is their location relative to the disc plane and its orbital motion direction relative to the disc rotation. The configuration parameters are shown in table 1 and a schematic illustration of all of them is represented in figure 2.1.1.

2.2. Simulations

Some of our simulations include star formation modeled as shown in ?. In this model a cold gas particle is able to convert part of its mass in stars when several criteria are met. Its temperature should be lower than 10^4 K and its density should be larger than a predefined threshold density (ρ_{th}). Additionally, the cooling time should be shorter than the col-

lapse time of the cloud $t_{\text{cooling}} < \frac{1}{\sqrt{G\rho}}$ and the local gas flow must be negative ($\nabla \cdot \vec{v} < 0$). These conditions guarantee that gas-rich regions, where the star formation process must happen, are colder, denser and undergoing collapse. Once a gas particle meets criteria to form stars, they are formed stochastically with a sampling determined by the local star formation rate. We refer the reader to ? for further details on the model and implementation of the star formation. Our goal is to study the possibility of formation of globular cluster-like structures in this kind of mergers. We are not interested in to study the process of star formation in these candidate structures since it will be very much dependent on the model and implementation of the different feedback mechanisms and star formation. Our interest introducing star formation and feedback in our simulations is to provide the gas with some sort of realistic conditions that can be meet for candidate structures to form.

As it is well known, SPH suffers from fragmentation instabilities that lead small gas clumps to cluster forming a set of non-physical structures (Bate

Name	Nomenclature	\mathbf{r}_0 (kpc)	\mathbf{v}_0 (km/s)
Perpendicular	<i>p</i>	(0,0,198.34)	(0,34.9,0)
Planar Corrotating	<i>pcr</i>	(0,198.34,0)	(-34.9,0,0)
Planar Contrarotating	<i>pct</i>	(0,198.34,0)	(34.9,0,0)
Inclined Corrotating	<i>icr</i>	(99.6,99.6,140.25)	(-24.67,24.67,0)
Inclined Contrarotating	<i>ict</i>	(99.6,99.6,140.25)	(24.67,-24.67,0)

TABLE 1

SPECIFICATIONS OF THE SATELLITE’S INITIAL ORBITAL CONFIGURATIONS CHOSEN FOR EACH SIMULATION. FOR A SCHEMATIC VIEW OF EACH CONFIGURATION, SEE FIGURE 4.

& Burkert 1997; Torrey et al. 2013). Since what we are looking for in our simulations is exactly fluctuations in the mass distribution we need to make sure that we find candidates that are not just spurious numerical fragments formed due to the SPH instability. In order to avoid this, we ran the same set of initial conditions for several different particle resolutions and we found that the substructures present in the lower resolution simulation were recognizable in the higher resolution simulations, maybe with a little spatial displacement due to changes in the global dynamics of the system as it can be seen in figure 13 (See section 3.2 to see how these substructures were identified). Increasing the resolution of the simulations allow us to verify that what we find as substructure candidates are true candidates and not numerical artifacts. Section 3.3 describes in better detail the results of our convergence study.

We design two sets of experiments to explore the formation of substructures in the tidal streams of the satellite galaxy. The first consists in pure collisionless systems, or in other words, gas-free simulations. The main purpose of these first experiment was to verify if the collisionless matter alone could cluster and form bound systems without the influence of gas. This set of simulations was named DMO (Dark Matter Only), specifically DMO1 and DMO2 whose only difference is the number of particles in the satellite as it is shown in Table 2 where we show the masses, number of particles and mass per particle of each galactic component in our models.

The second set of simulations included gas in the satellite and were designated with the nomenclature GAS. The difference among them is the increased resolution, being GAS3 the one with the highest resolution. Table 2 summarizes the resolution specifications of the GAS experiment.

As it can be seen in table 2 the SPH particle mass is of the order of $5 \times 10^3 h^{-1}M_\odot$ for GAS3. If we assume that typical masses for globular cluster candidates are of the order of 10^5 to $10^7 h^{-1}M_\odot$ in this simulation we could resolve globular cluster like structures with between 20 to 2000 gas particles. Again, we are not interested in to study star formation in those objects (which will imply the necessity of larger resolution simulations in order to sample properly star formation inside the clusters) but study the collapse of gas in the candidate structures, therefore these numbers are good enough for the purposes of our work. Finally, we have ran our simulations during a time interval of the order of 7 Gyr, long enough to study the evolution of the satellite remnants as it would be observed in present time.

3. ANALYSIS

3.1. Density Estimation

Overdensities are, by definition, regions with a spatial mass density that is larger than its surroundings. Hence, the best way to identify them is by estimating the mass density in the body of the tidal streams. High density regions will be the best candidates to form autogravitating substructures. We used the EnBiD (Entropy Based Binary Decomposition) algorithm to calculate the density distribution in real and phase spaces (Sharma & Steinmetz 2006).

The EnBiD algorithm is sensitive to the spatial anisotropies of the mass distribution by the implementation of the anisotropic smoothing tensor. In this way, any density underestimation is prevented due to the ability of the method to use particles along a preferred direction and not only spherically symmetric around the point of interest, as the isotropic kernels do. Figure 5 shows the estimated density for the total number of particles in one of the GAS simulations at $t = 3.75$ Gyr. In the figure we show the

COLLISIONLESS SIMULATIONS				
Name	Component	Mass (M_{\odot})	N_p	m_p (M_{\odot})
DMO1	Satellite	3.2×10^{10}	1.0×10^5	3.2×10^5
	Disk	3.3×10^9	5.6×10^4	6.4×10^4
	Halo	7.9×10^{11}	7.3×10^5	1.1×10^6
DMO2	Satellite	3.2×10^{10}	2.0×10^5	1.6×10^5
	Disk	3.3×10^9	5.6×10^4	6.4×10^4
	Halo	7.9×10^{11}	7.3×10^5	1.1×10^6
COLLISIONAL SIMULATIONS				
Name	Component	Mass (M_{\odot})	N_p	m_p (M_{\odot})
GAS1	Satellite	2.5×10^{10}	4.0×10^5	6.2×10^4
	Gas	5.0×10^9	2.0×10^5	2.5×10^4
	Disk	3.3×10^9	5.6×10^4	6.0×10^4
	Halo	7.9×10^{11}	7.3×10^5	1.1×10^6
GAS2	Satellite	2.5×10^{10}	8.0×10^5	3.1×10^4
	Gas	5.0×10^9	4.0×10^5	1.2×10^3
	Disk	3.3×10^9	5.6×10^4	6.4×10^4
	Halo	7.9×10^{11}	7.3×10^5	1.1×10^6
GAS3	Satellite	2.5×10^{10}	3.0×10^6	8.3×10^3
	Gas	5.0×10^9	1.0×10^6	5.0×10^3
	Disk	3.3×10^9	5.6×10^4	6.4×10^4
	Halo	7.9×10^{11}	1.0×10^7	7.9×10^4

TABLE 2

COLLISIONLESS AND COLLISIONAL SIMULATIONS DATA. N_P AND M_P ARE THE NUMBER OF PARTICLES AND MASS PER PARTICLE RESPECTIVELY.

density of gas, halo dark matter, disk and satellite particles. New stars formed from gas particles are also included. Note that this figure only shows the densities of particles ranked by ID (and type) but allows to see the high density peaks. As we know, these density peaks are associated to gravitational instabilities and should be related to anisotropies in the density distribution of each galactic component, therefore, an adequate density threshold can be selected to extract the prominent overdensities in the particle distribution.

As it can be seen in the figure, the overall density of the halo, disk and a fraction of particles of the satellite have a lower density value than that for a fraction of particles of gas and stream material (which in this case corresponds to the last bump composed of satellite particles and new born stars). The peaks in the values of the estimated density can be used to fix a density threshold ρ_{th} that can be used to identify global overdensities, as it is shown by the horizontal line in figure 5. Notice that only a fraction of gas, satellite and new star particles

are above this threshold, and one expects that since those overdensities are induced by gravitational instability, they are spatially correlated, as it can be seen in figure 13. This density threshold is an important part of the process of identification of high density peaks corresponding to the seed of the identification of potential cluster candidates.

3.2. Identification of Substructure Candidates

Once the densities of the particles have been calculated, we aimed to identify the overdensities in the field of the stream in order to label them as possible candidates. We start by estimating density maps as described in the previous section. These maps highlight the overdensities above the underlying distribution of particles as it is shown in figures 10 and 11. Then, the identification is carried out by the following series of steps:

- First the candidates are identified by performing a selection of particles through a phase space density threshold ρ_{th} . Particles with phase-space densities below the density threshold are

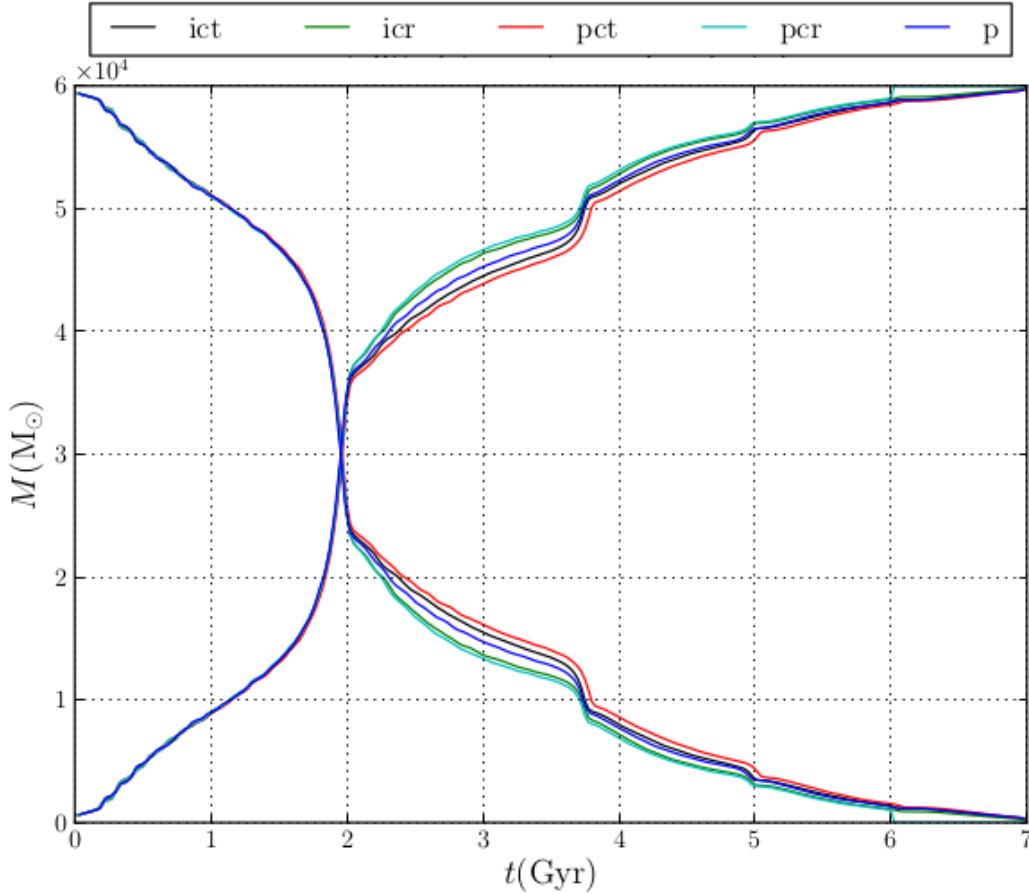


Fig. 6. Mass stripped out from the satellite galaxy as a function of simulation time represented by the descending curves for each orbital configuration. The mass gained by the stream for each orbital configuration are the ascending ones.

ruled out as potential center of some candidate clump. The value of ρ_{th} was chosen examining the values of the density of the simulation using, for instance, a plot like the one shown in figure 5 in which we clearly distinguish between particles of high and low density. The density threshold could be different from one simulation to another.

- Once the particles with $\rho < \rho_{\text{th}}$ are ruled out, we elaborate a three dimensional spatial plot of the particles that are left. In this plot, it is identified, *by eye* a centre of each overdensity. The coordinates of the centre at that particular snapshot are then estimated to be $\mathbf{r}_c = (x_c, y_c, z_c)$. We chose a random snapshot to do this procedure, but it is preferable that the system has had an important evolution, maybe after the satellite has passed several times through the disk. The fact that at this point we choose by hand

the position of the candidate has no effect on the results. Using for example a method like spherical overdensity would work equally well since we are just finding a guess for the position of the overdensity.

- Based on the three dimensional plot built before, it can be roughly estimated the size of the overdensity. We assign a spherical radius R_0 , measured from the centre \mathbf{r}_c , trying to encompass the largest number of overdensity particles. Then, particles with position $\mathbf{r}_p = (x_p, y_p, z_p)$, which meet the condition $|\mathbf{r}_p - \mathbf{r}_c| < R_0$ are said to be in the first guess of the candidate list. After inspection, we have found that using a value of $R_0 \sim 2.0$ Kpc was enough to encompass all initial particles in each substructure that will be used later to track the actual set of bound particles.
- With the ID number of each particle in the can-

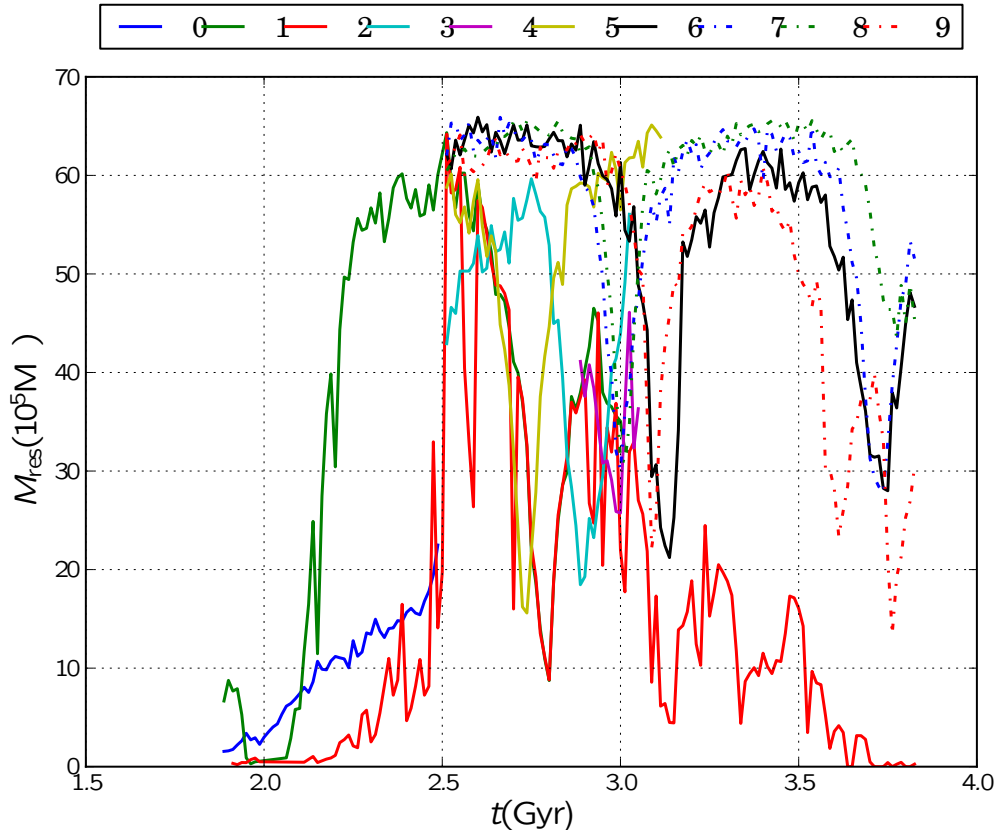


Fig. 7. Minimum resolvable masses for the nine candidates in GAS3 (equation 6). The minimum mass remain much smaller than the candidates total mass, see figure 9.

candidate list, we track the position and velocities of such particles in all the snapshots in the simulations. At this point, we compute the center of mass of the particles in the candidate (for each snapshot) and look for particles of any kind that lie within a sphere of radius $R_{th} = 0.7\text{Kpc}$, including dark matter particles from the host and the satellite halos, gas, disk particles and new stars born during the interaction. Notice that across the snapshots particles can come in and out of the sphere of $R_{th} = 0.7\text{Kpc}$ in a way that the list of particles that actually belong to the candidate has to be updated dynamically.

- Then, for every snapshot, we compute the properties of the clump in order to inspect the evolution of the visually identified clouds with an astrophysical observed system. Such properties are center of mass, energy binding, total mass, the mass by type of particle, central and mean densities, tidal and core radii and the tidal heating.

3.3. Resolution Study Against Artificial Fragmentation

The numerical scheme used to simulate the hydrodynamics of the gas could impact the formation of clumps within the molecular clouds in an artificial way. The resolution of a SPH simulation involving gravity is therefore a critical quantity in order to obtain realistic results from physical process rather than artificially induced mechanisms by numerical fluctuations.

As it is widely known, in SPH the properties of gas particles are obtained by summing the properties of all the particles that lie within a sphere with a radius known as the smoothing length h . The smoothing lengths are constrained to contain approximately a number of particles, called number of neighbours N_{ngb} , in the sphere of radius h . Since the gravitational softening is set equal to h , the mass contained in the sphere can not be roughly equal to the local Jeans mass, otherwise the collapse is inhibited by the softening of the gravitational forces.

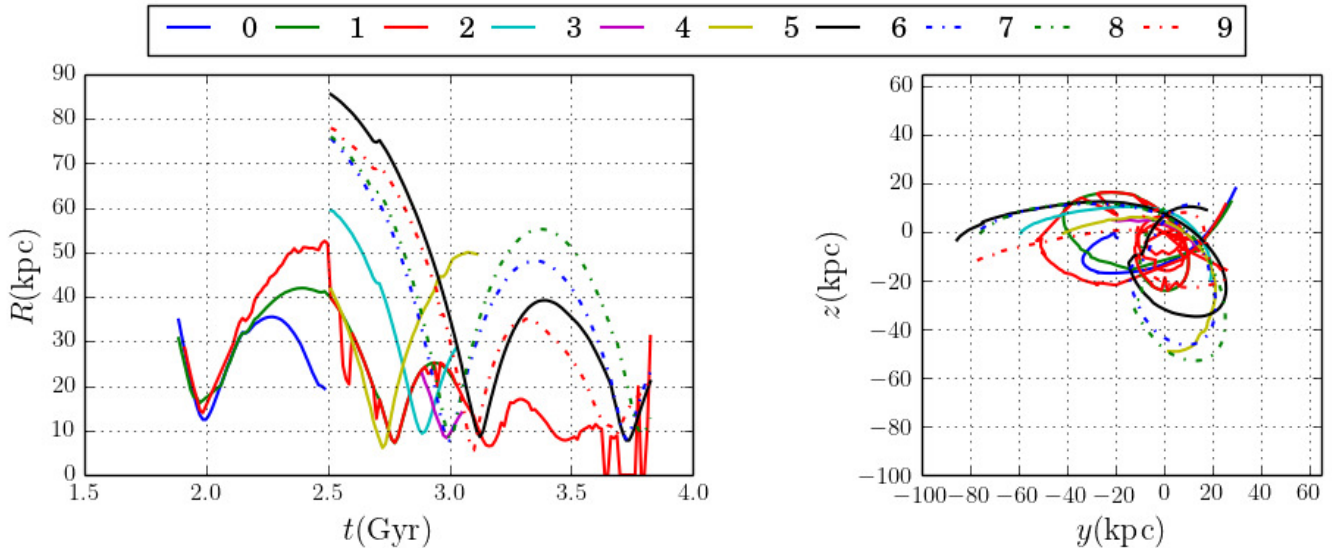


Fig. 8. Orbital structure of the nine candidates identified in GAS3. *Left panel*, Magnitude of the galactocentric vector position as a function of time. *Right panel*, Projection of the orbits in the $y - z$ plane.

Thus, the called *minimum resolvable mass*, M_{res} must always be less than the local Jeans mass M_J given by

$$M_J = \left(\frac{3}{4\pi\rho} \right)^{1/2} \left(\frac{5k_B T}{\mu m_H G} \right)^{3/2}, \quad (5)$$

where ρ is the density of the gas at temperature T , k_B is the Boltzmann constant, m_H is the mass of the hydrogen atom and μ is the gas mean molecular weight (Draine 2011). Taking M_{res} as the mass of $2N_{\text{ngb}}$ particles, it can be estimated as Bate & Burkert (1997)

$$M_{\text{res}} = M_{\text{gas}} \left(\frac{2N_{\text{ngb}}}{N_{\text{gas}}} \right), \quad (6)$$

where M_{gas} and N_{gas} are the total mass and particle number of the gas. The previous expression explicitly shows that for a larger number of particles, the minimum resolvable mass decreases and the collapse and fragmentation will be less affected for the numerical implementation.

The condition (6) with $N_{\text{ngb}} = 128$ is tested for the clumps in the satellite galaxy gas that we selected as substructure candidates with the previous recipe. The strategy adopted for the identification of the progenitors and the results obtained of such strategy are depicted in the next sections.

Figure 7 shows the time evolution of the minimum resolvable mass for each cluster according to 6,

which remains much smaller than the local Jeans mass.

4. RESULTS

In figure 6 we show the mass stripped out from the satellite galaxy as a function of simulation time. Each line in figure 6 represents the evolution of the mass stripped out from the satellite for each of the five orbital configurations presented in table 1. As it can be seen in the figure, the rate of mass loss is quite similar for every orbital configuration of the merger. For this reason, since in our experiments we found no reason to prefer an orbit from any other, on the basis of the amount of mass stripped out of the satellite, we decided, without loss of generality, to run our high resolution simulations only for the configuration of the orbit perpendicular to the plane of the galaxy.

As it can be seen in the figure, there are breaks in the mass curve located at 2, ~ 3.8 and 5 Gyr. These breaks are associated with the periastron passages during the merger. Clearly it is the first passage the one stripping the largest amount of mass out from the satellite. Most of the mass ejected during the first passage is gas that is heated up during the collision and should remain bounded to the host galaxy potentially forming overdensities that we are interested in our study.

Figure 10 shows the projected particle distribution of the DMO2 simulation at two different time snapshots, $t = 6$ Gyr and $t = 7$ Gyr. The figure

shows (at the top) in color coded the density the streams where it can be seen the umbrella effects associated to the distribution of the merger remnant of a satellite interacting with a massive host galaxy. At the bottom, each figure shows the pseudo phase space diagrams, where it can be seen the disturbances in phase space associated to the structures of the streams and merger remnants. As it can be seen at the two different time snaps, there is a diffuse structure that appears at the time 6Gyr (in real space and phase-space) but that after 1Gyr is already washed out. This happens to all structures observed in the simulations with only collisionless matter.

Figure 11 shows the same projected particle distribution coded with density colour as the figure 10 but for the GAS2 simulation. Unlike the case exposed in the previous paragraph, as it is clear from the projected density and phase-space density, there are more overdensities and they survived for several orbital periods keeping their structure for a significant lifetime fraction. Figure 12 shows a zoom of the inner region of figure 11 near the galactic disc. From this result, constrained by the resolution of our DMO simulations, we conclude that to form long lasting structures we need cold gas that helps to keep particles bounded gravitationally.

GAS simulations are thus the ones with better results in the formation of stream substructures. Consequently, we targeted them to apply the algorithm for identification of substructure candidates whose results are shown in figure 13 where the galactic disc of the host galaxy is also shown as a reference. The plots show the candidates identified in the simulations GAS1, GAS2 and GAS3 for the same simulation time of 3 Gyr for comparison purposes. It is clearly evident that the higher resolution simulation has the greater number of substructures, which in turn, have the highest number of particles among all the simulations of this work. For this reason we only study the properties of the substructures of GAS3.

For each substructure identified in the simulation we investigated several properties. In GAS3 were identified 10 overdensities associated to the 10 most densest peaks that we label with numbers from 0 to 9 and for each one of them we start by determining their orbital evolution. Figure 8 (b) shows the $y - z$ projection of the orbit of the center of mass followed by each candidate. Figure 8 (a) shows the distance between each candidate to the center of the disk of the host galaxy as a function of time. The more notable aspect of this plot relies in the fact that the candidates persist among a significant amount of time, with life times that are of the order of 1Gyr or

longer.

Figure 9 shows the evolution of the mass content of each candidate in GAS3. For all the candidates, the principal constituent is gas. The high peaks of host dark matter content present in the candidates are circumstantial particles that are counted by the algorithm when the candidate traverses the central region of the dark halo where the density is sufficiently high to cause the miscounting of host dark particles as candidate particles. The masses found in each candidate correspond to the masses measured for globular clusters and high-velocity clouds, both ranging from $10^3 M_\odot$ to a maximum of $10^6 M_\odot$ in average, although there are several cases of clusters with masses above of the $10^6 M_\odot$ value (Harris 1999; Wakker & van Woerden 1997).

4.1. Dark Matter in Cluster Candidates

The candidate labeled as Candidate 0 was the only formed by gas and particles of another species. Figure 9 (a) clearly shows that the predominant mass component is the dark matter of the satellite from where it comes. This dark matter component is not circumstantial, and is an important part of this candidate during its lifetime. The rest of the candidates are basically cores of gas, without dark matter or disc stars. This suggest that through this formation mechanism one could expect to find dark matter in globular cluster.

5. SUMMARY AND DISCUSSION

In this work we used N -body simulations of satellite galaxies undergoing minor merger with a larger host galaxy. Our goal is to find if there is formation of globular cluster-like systems in the tidal stream formed by the tidally stripped material from the satellite. The work was divided in two main parts: The first part was performed to explore the possibility of formation of structures from pure collisionless simulations, the second part was dedicated to simulate the formation of cluster-like structures from mergers that included gas.

Then we performed several estimations in the simulations to identify the stream and the possible autogravitating substructures inside it. The approach adopted to identify substructures was the estimation of the phase-space density which reveal the presence of substructures as density peaks.

The density estimation clearly identifies overdensity regions in which a cluster-like structure could be formed. As a first conclusion we argue that without gas, the substructures that could be formed (if at all) have a sort life as none of the overdensities show

a definite morphology or stability over time. When the gas was included, several clumps appear.

Running with gas physics results are remarkably different. The candidates identified in the simulation proved real physical structures that lived for a considerable amount of time and whose orbital evolution leads them to be objects in the surroundings of the galactic disk. The total absence of stars formed within the clumps is mainly due to the thermodynamic setup of the gas as an initially isothermal sphere, the temperature of the gas is high enough that inhibits instantaneous star formation in the candidates. Another factor at play is the implementation/parameters of the feedback we used in the simulations that made the effect of feedback to be a bit to strong in the satellite galaxy. (Oppenheimer & Davé 2006) discuss that the original implementation of (Springel & Hernquist 2003) does not work equally well for all halo masses and the model and the parameters should be somehow mass dependent. As it was already mentioned, due to all the physics involved in the problem of star formation in this kind of complex scenarios, it is out of the scope of this work to study star formation in these candidate structures.

The main conclusion of this work is that substructures (globular clusters and high velocity clouds) could be formed in tidal streams of gas rich satellites. The validity and scope of this main conclusion should be tested by running simulations with higher resolutions and taking in to account different feedback and star formation models. This is the road map for future work that contributes to improving and supplementing the results presented here.

Certainly our experiments are limited. First of all, we could study all other orbital configurations to complement the study. However, having found that one of the merger configurations already produced the formation of candidate clusters, the goals of our work where already meet. Studying under which conditions (merger orbits) it is more easy to form this kind of structures is an interesting idea, but indeed it would require a larger amount of computing time in order to run a suite of simulations to develop the idea.

We could have included gas in to the disk of the host galaxy, we could also have included a hot gas halo in to the main galaxy (we did not do it because it made the simulations much more expensive). Both aspects are important because these gaseous components could affect the dynamics of the merger and the dynamics of the gas in the stream through ram pressure stripping and shock heating. Both pro-

cesses could work stripping more gaseous material from the satellite, making larger the amount of gas in the stream, so, we expect it will contribute to increase the fraction of gas that could end up falling in to cluster candidates. However the limited design of our experiment shows to suffice to answer the question on the formation of candidate globular cluster structures in this kind of processes and we expect that including those other gaseous components are not going to change the main conclusions of the work.

Acknowledgments

Research work was supported by COLCIENCIAS (doctorados nacionales, convocatoria 617 de 2013) and the project 111571250082 (convocatoria 715-2015). N.I.L acknowledges financial support of the Project IDEXLYON at the University of Lyon under the Investments for the Future Program (ANR- 16-IDEX-0005). Additionally, simulations performed in this work were run in the computer facilities of GFIF in the Instituto de Física, Universidad de Antioquia, Hipercubo in the Instituto de Pesquisa e Desenvolvimento (IP&D-Univap), Leibniz-Institut Für Astrophysik Potsdam. The authors gratefully acknowledge the Gauss Centre for Supercomputing e.V. (www.gauss-centre.eu) for funding this project by providing computing time through the John von Neumann Institute for Computing (NIC) on the GCS Supercomputer JURECA at Jülich Supercomputing Centre (JSC). Finally, L.F.Q. & D.A.N. thank Mario Sucerquia for his meaningful comments in the preparation of the paper.

REFERENCES

- Ashman, K., & Zepf, S. 1992, *ApJ*, 384, 50
- Bate, M. R., & Burkert, A. 1997, *MNRAS*, 288, 1060
- Bekki, K., & Chiba, M. 2002, *ApJ*, 556, 245
- Bekki, K., & Freeman, K. 2003, *MNRAS*, 346, L11
- Belokurov V., et al., 2006, *ApJ*, 642, L137
- Binney, J. & Tremaine, S. *Galactic Dynamics*, 2008, Princeton University Press
- Binney, J., Nipoti, C. & Fraternali F. 2009, *MNRAS*, 397, 1804
- Blitz L., et al. 1999, *ApJ*, 514, 818
- Carroll, B. W., & Ostlie, D. A, *An Introduction to Modern Astrophysics*, 2008, Addison-Wesley
- Conroy C., et al. 2011, *ApJ*, 741
- Draine, B. T. *Physics of the Interstellar and Intergalactic Medium*, 2011, Princeton University Press
- Elmegreen, B. G., & Efremov, Y. N. 1997, *ApJ*, 480, 235
- Forbes, D. & Bridges, T. 2010, *MNRAS*, 404, 1203
- Forero-Romero, J. E., et al. 2010, *MNRAS*, 417, 1434
- Fraternali F., et al., 2015, *MNRAS*, 447, L70
- Georgiev I. Y., Puzia T. H., Goudfrooij P., Hilker M., 2010, *MNRAS*, 406, 1967

- Gottloeber, S., Hoffman, Y., & Yepes, G. 2010, arXiv:1005.2687
- Harris, W. E. *Globular Clusters Systems*, 1998, Springer
- Harris, W. E. 1999, 10th Canary Islands Winter School of Astrophysics: Globular Clusters, 325
- Hernquist L. 1993, MNRAS, 86, 389
- Ibata R., et al., 2001, ApJ, 551, 294
- Kúpper, A. H. W., Lane, R. R., & Heggie, D. C. 2012, MNRAS, 420, 2700
- Li, Y., Law, M., & Klessen, R. 2004, ApJ, 614, L29
- Lin L., et al., 2008, ApJ, 681, 232
- Mastropietro, et al. 2005, MNRAS, 363, 509
- Mo, H. J., Mao, S., White, S. D. M. 1998, MNRAS, 295, 319
- Monaghan J. 1992, Annual Review of Astronomy and Astrophysics, 30, 543
- Moster et al. 2001, ApJ, 710, 903
- Norris, M.A. & Kannapan S.J. 2011, MNRAS, 414, 739
- Oppenheimer B. D., Davé R., 2006, MNRAS, 373, 1265
- Peebles, P.J.E, & Dicke R.H. 1968, ApJ, 154, 891
- Price-Whelan A., et al 2018, Submitted to ApJ
- Reina-Campos M., et al 2019, MNRAS, 486, 5838-5852
- Shapiro K. L., Genzel R., Förster Schreiber N. M., 2010, MNRAS, 403, L36
- Sharma S. & Steinmetz, M. 2006, MNRAS, 373, 1293
- Springel V. 2005, MNRAS, 364, 1105
- Springel V., White, S. D. M. & Hernquist L. 2004, International Astronomical Union Symposium, 421
- Springel, V., & Hernquist, L. 2003, MNRAS, 339, 289
- Springel V. & Hernquist, L. 2002, MNRAS, 333, 649
- Torrey, P., et al. 2013, ASP Conference Proceedings, 477, 237
- Wakker, B. P., & van Woerden, H. 1997, Annual Review of Astronomy and Astrophysics, 35, 217
- Wetzell, A. R. 2011, MNRAS, 412, 49
- Zepf, S. & Ashman, K. 1993, MNRAS, 264, 611

FACom - Instituto de Física, FCEN, Universidad de Antioquia (UdeA), Calle 70 No. 52-21, Medellín, Colombia.
(†david.norena@udea.edu.co).

Leibniz-Institut für Astrophysik Potsdam (AIP), An der Sternwarte 16, D-14482 Potsdam, Germany.

l'Institut de Physique Nucléaire de Lyon (IPNL), University of Lyon; UCB Lyon 1/CNRS/IN2P3; Lyon, France.

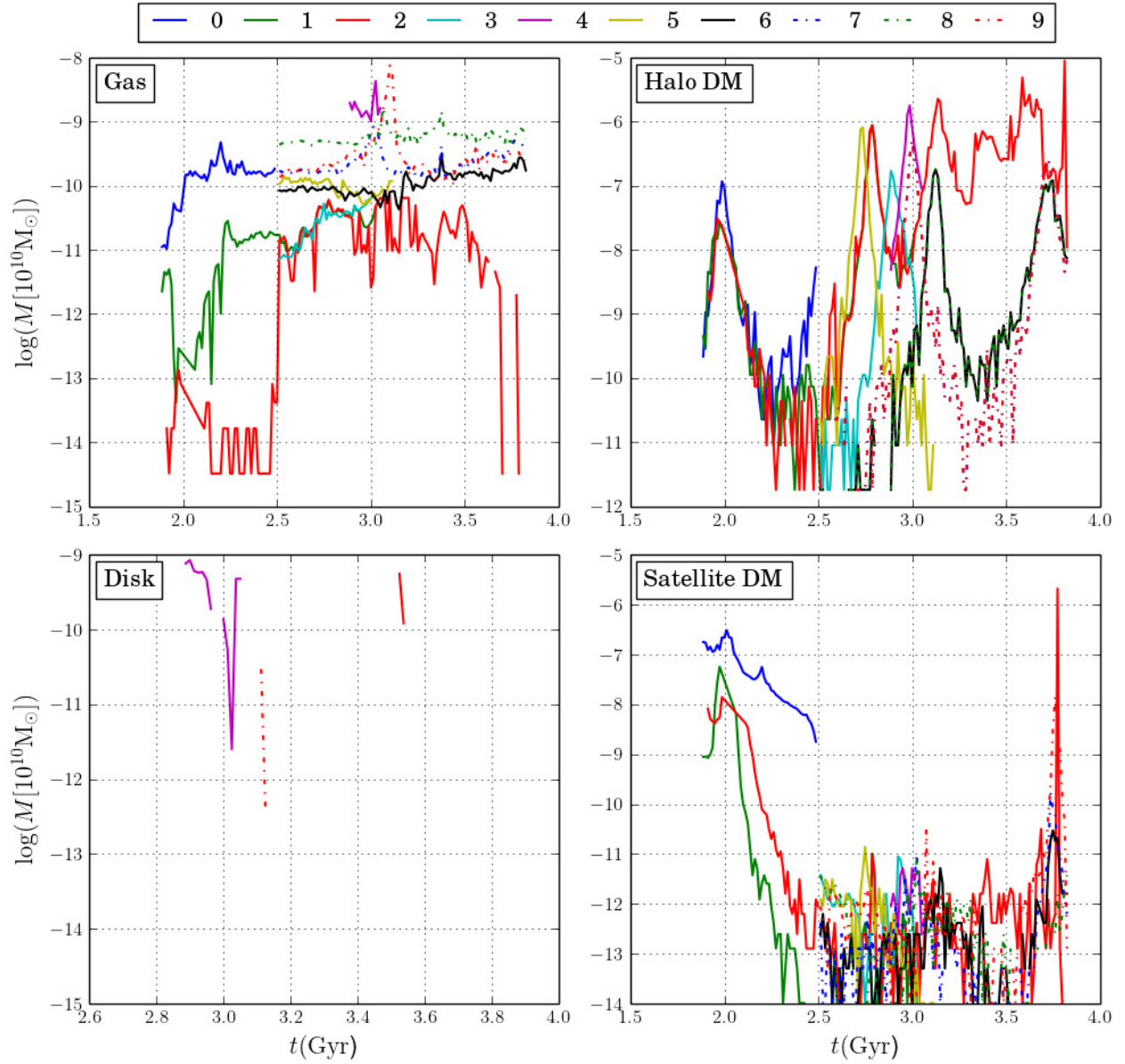


Fig. 9. Mass as a function of time for each candidate, segregated by type.

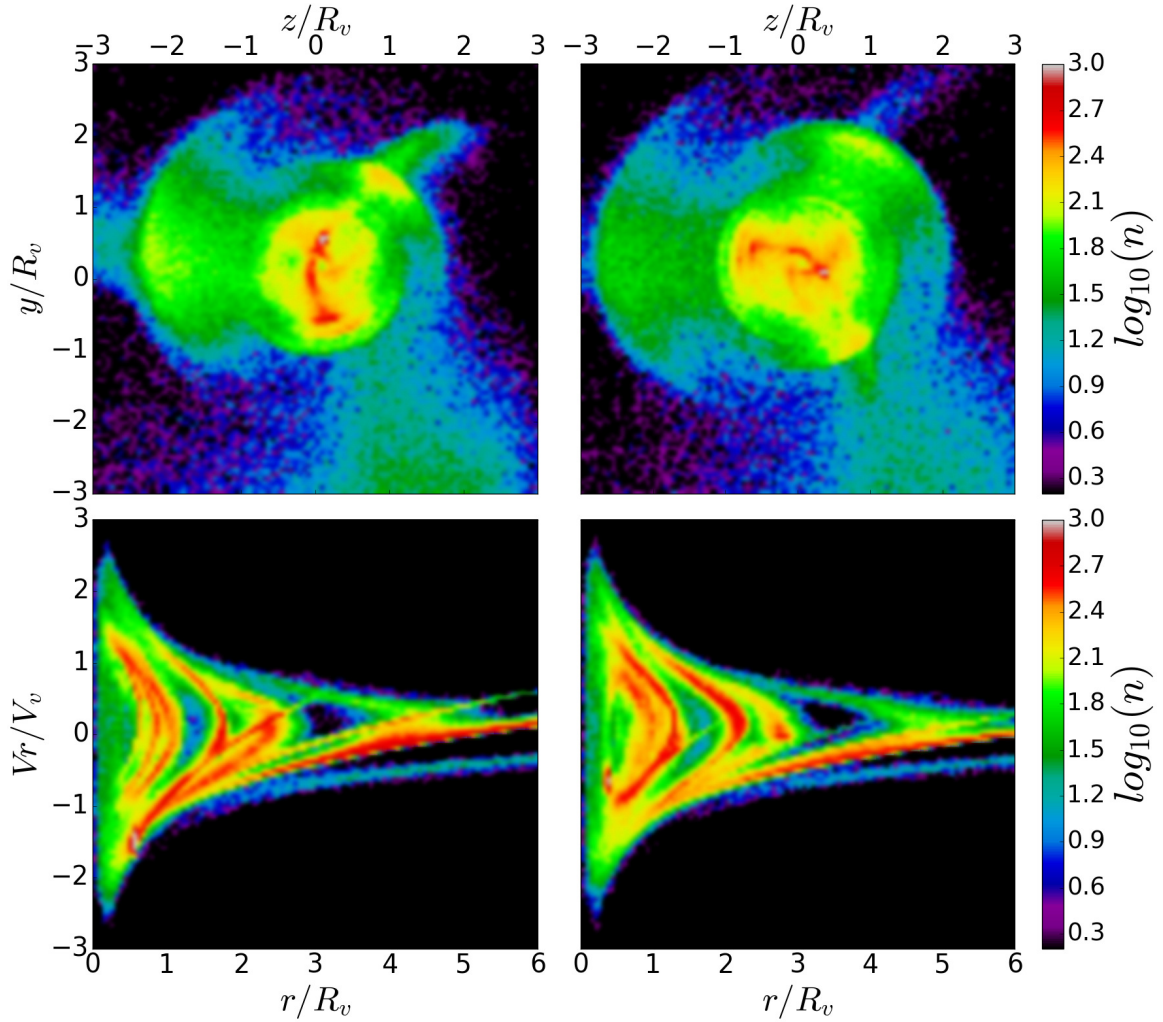


Fig. 10. *Top Panels:* Real space projection on the $z - y$ mapped with density for DMO2 simulation. *Bottom Panels:* Phase space projection on the $r - v_r$ plane with same density color mapping. The density contrast is high in the the elongated radial structures found in the tidal tails, but still do not exhibit the morphology of globular clusters. Pannels at the left correspond to a time of 6.0 Gyr while right panels are at 7.0 Gyr. Color values correspond to number density of points in log scale.

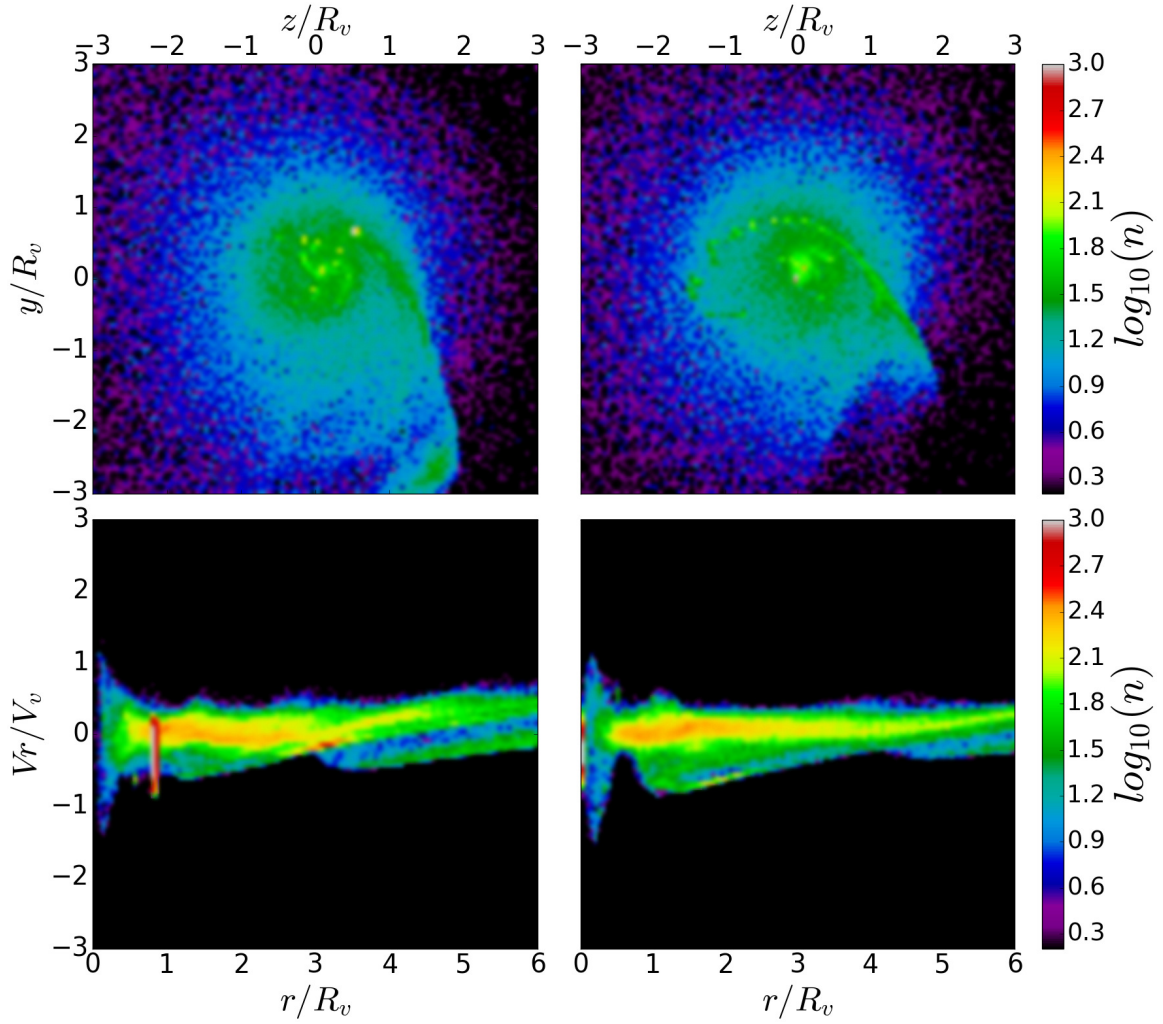


Fig. 11. *Top Panels:* Real space projection on the $z - y$ mapped with density. *Bottom Panels:* Phase space projection on the $r - v_r$ plane with same density color mapping. R and V are the virial radius and velocity respectively. This corresponds to a couple of snapshots of GAS2. Panels at the left corresponds to a time of 5.00 Gyr while rith panels are at 6.25 Gyr. Color values correspond to number density of points in log scale.

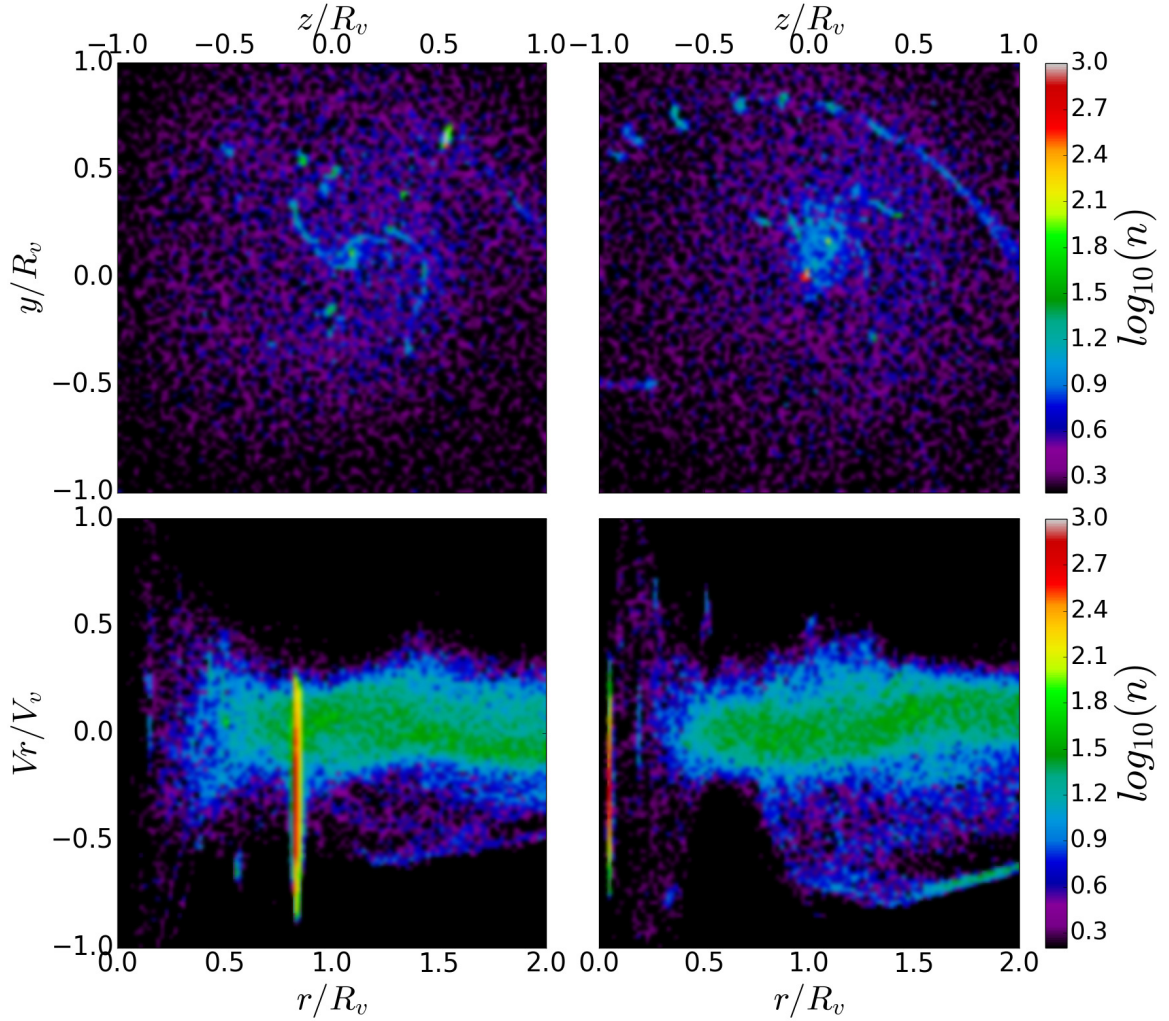


Fig. 12. *Top Panels:* Real space projection on the $z - y$ mapped with density. *Bottom Panels:* Phase space projection on the $r - v_r$ plane with same density color mapping. This plot is exactly figure 10 but zooming to the internal region near the galactic disc for GAS2. Panels at the left correspond to a time of 5.00 Gyr while panels at the right are at 6.25 Gyr. Color values correspond to number density of points in log scale.

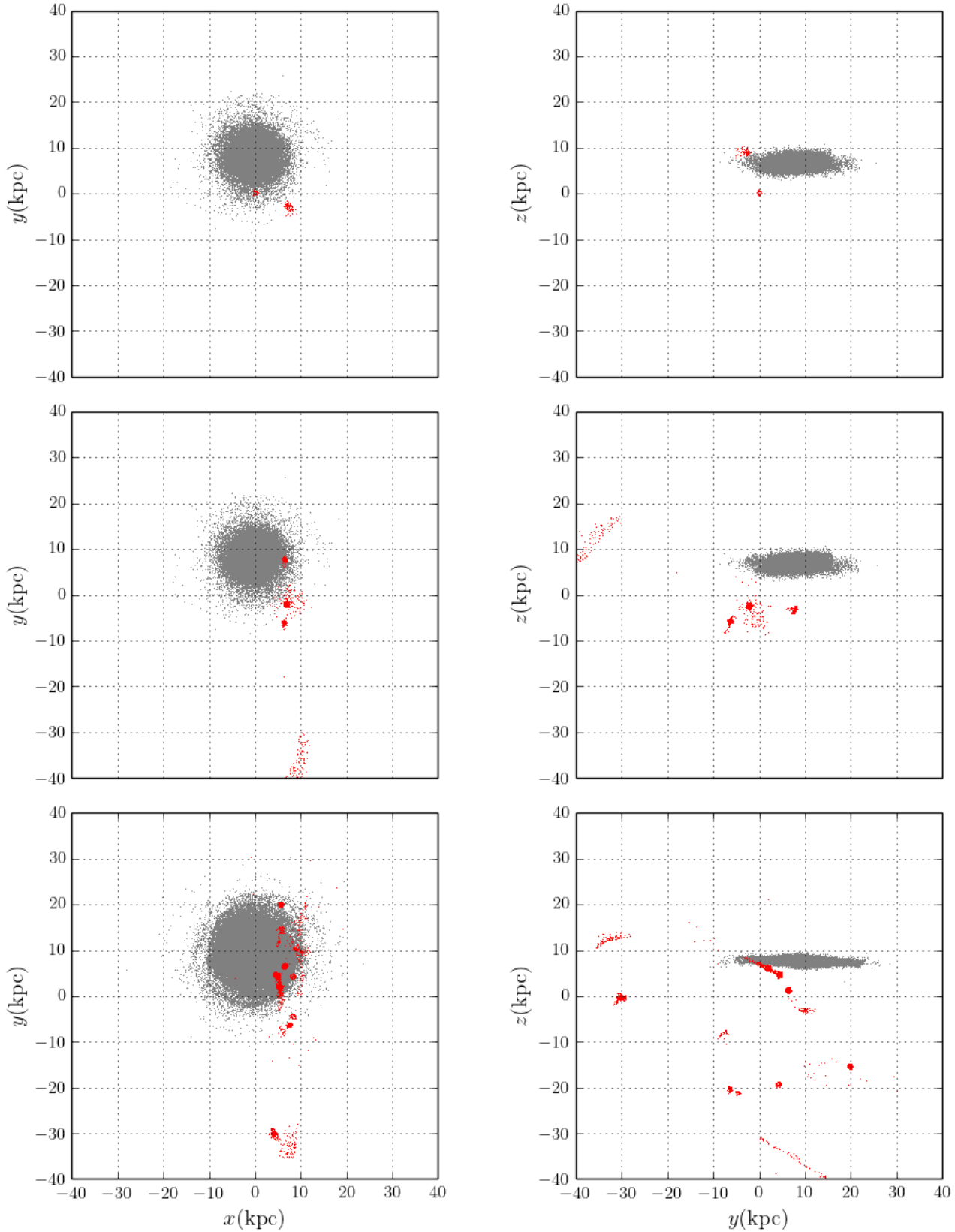


Fig. 13. Candidates identified with the algorithm described in section 3.2. The number of clumps increase with increasing resolution. All plots correspond to 3 Gyr simulation time. *Top row*, shows the candidates in GAS1. *Middle row*, candidates in GAS2. *Bottom row*, candidates in GAS3. In each row, at the *left*, the disc is seen face on, and at the *right*, the disc is seen edge on.